Computer simulation of adsorption on nanoparticles: The case of attractive interactions

O. A. Pinto,[1] B. A. López de Mishima,[1] E. P. M. Leiva,[2] and O. A. Oviedo[2,*]

[1]*Centro de Investigaciones y Transferencia de Santiago del Estero, Universidad Nacional de Santiago de Estero, RN 9 Km 1125 Villa el Zanjón, Santiago del Estero, CP 4206, Argentina*

[2]*Instituto de Fisicoquímica de Córdoba, Departamento de Matemática y Física de la Facultad de Ciencias Químicas, Universidad Nacional de Córdoba, Córdoba X5000HUA, Argentina*

(Received 4 June 2012; revised manuscript received 12 October 2012; published 10 December 2012)

A lattice-gas model describing adsorption on nanoparticles of different sizes and shapes is proposed and the adsorption thermodynamics is studied. The nanoparticle is modeled assuming different geometries, and Monte Carlo simulations are performed in the grand canonical ensemble. Adsorption isotherms, differential heats of adsorption, and other relevant thermodynamic properties are analyzed as a function of nanoparticle sizes. The simulations cover a wide range of interactions, ranging from physical to strong chemical bonds.

DOI: 10.1103/PhysRevE.86.061602 PACS number(s): 68.35.Md, 68.35.Rh

I. INTRODUCTION

In recent years, nanometric systems have become the subject of numerous experimental and theoretical studies because of their important implications for physical chemistry, biology, and medicine, just to name a few fields [1–3]. The special behavior of systems made of a relatively small number of particles was recognized in the 1960s by Hill [4,5], who described the basis of the thermodynamics that he called "of small systems." Hill described in a visionary way how size could affect various thermodynamic properties of these systems. Keeping the pace of "nano times," this theoretician extraordinarius [6] gave this area of study a new name; he called it nanothermodynamics [5].

Since relative fluctuations are small in macroscopic systems, different ensembles can be chosen to deal with a given problem, on the basis of mathematical or physical convenience. However, this may not be valid for a nanosystem [7], so it becomes necessary to specifically derive the equations for each ensemble. Thus, if a joint approach to a given problem involving theory, simulations, and experiments is attempted, it is necessary that both the theoretical modeling and the simulations reflect the experimental conditions. Another remarkable feature of nanothermodynamics is that we have to abandon the macroscopic concept of intensive and extensive variables. In nanothermodynamics, some of the properties that in the macroscopic limit did not depend on the system size now will depend on it [4,5,7].

In the present work, the nanosystem in which we are interested is a nanoparticle (NP) on which atoms (eventually molecules) may be adsorbed from a source providing them at a constant temperature and chemical potential. A NP is a cluster of atoms that qualifies as a "small" system, in the sense considered by Hill, because it is composed of a few hundred (at the most a few thousand) units.

Among experimental studies, the use of electrochemical techniques [8] has opened the possibility of controlling the shape of Au NPs via the presence of other metallic adsorbates. In electrochemical systems, the coverage degree of adsorbed species may be controlled by straightforward application of a potential difference, which may be achieved by an electrode or via a redox system in equilibrium with the NP [9]. Thus, the interesting point about electrochemistry is that the adsorption-desorption equilibrium may be established without the need of application of high temperatures to the system, that would otherwise change the properties of the NPs.

Computer simulations have been widely used to simulate the generation of metallic and bimetallic NPs and to study their thermodynamic properties [7,10]. As an example, bimetallic NPs have been analyzed with a dynamic method to generate NPs by collision [11,12] or for the study of the electrochemical generation of core-shell NPs [13]. In these works, the thermodynamics properties can be affected by factors such as size and shape of the core, and chemical composition and under- or oversaturation conditions. Most of these simulations involve the use of many-body potentials and off-lattice models, which are expensive from a computational viewpoint. An appealing alternative to circumvent this problem may be the use of lattice models, where the particles of the system may be assumed to occupy a discrete position in space. This approach has been used successfully in a number of studies of supported NPs [14–17] to consider the change in the shape and surface morphology of the NP under the influence of the reaction media.

The icosahedral morphology is frequently found in experiments using the vapor condensation method with helium, where the particles are supported [18]. Icosahedral clusters have also been used to study melting of clusters by means of molecular dynamics simulations [19], with the finding that this structure is often stable up to the melting temperature.

The purpose of the present work is to study the thermodynamics of monolayer formation on a NP of fixed size by grand canonical Monte Carlo (GCMC) simulations in a lattice model approximation. The paper is organized as follows. Section II describes the lattice-gas model and some basic definitions. Section III shows the results for the thermodynamic behavior obtained from GCMC simulations. Finally, in Sec. IV the conclusions and future perspectives are given.

II. MODEL AND BASIC DEFINITIONS

In order to consider the deposition of different particles on a preexisting substrate (seed-NP), we define a lattice-gas model emulating a substrate with given geometry, formed by atoms

*Corresponding author: ooviedo@fcq.unc.edu.ar

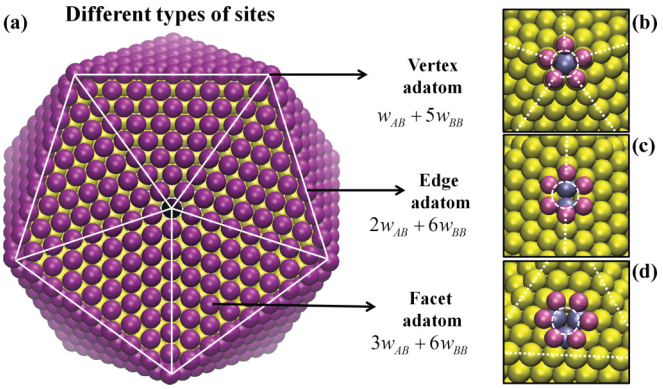

FIG. 1. (Color online) Representation of the lattice model used in this work. The purple atoms correspond to the adsorbates. The edge and vertices sites are marked in white solid lines in (a). Yellow atoms correspond to atoms of the substrate. Gray atoms in (b)–(d) correspond to atoms of the substrate that are coordinated with the adsorbate particles. The straight broken white lines are drawn to indicate the location of the edges. The circles drawn indicate the adsorption site of a particle that corresponds to a vertex (b), an edge (c), or a facet (d).

of type A on which the particles of type B are deposited. The NP will be denoted by the numbers of constituting particles, say N_A and N_B (N_A/N_B). The NP is assembled in such a way that each particle is linked to others if the distance between them is less than (or equal to) 1.2 times the nearest-neighbor distance of the bulk A species. The M adsorption sites for the B adsorbates are located on the surface of the seed NP. We note that M depends on the preexisting NP size and shape.

Taking into account the coordination with nearest neighbors, different types of adsorption sites occur where the particles can be deposited. Figure 1 shows a schematic view of the different types of sites and their coordination numbers for the particular case of icosahedral geometry. The adsorption sites on the faces of the icosahedrons [Fig. 1(d)] are linked to three atoms of the substrate, forming a triangular lattice capable of coordinating with up to six lateral neighbors on the surface. The adsorption sites on the edges [Fig. 1(c)], are linked to two sites of the substrate and may coordinate with up to six other adsorbate sites. Finally at each of the twelve vertices [Fig. 1(b)], the adsorption site is connected to one site of the substrate and with up to five lateral nearest neighbors. Following these ideas we can consider two different kinds of interaction energies. One between A-type and B-type particles, denoted with w_{AB} and another one corresponding to the lateral interaction between B-type particles, say w_{BB}. Thus, the surface of the NP forms a heterogeneous substrate on which foreign particles are deposited. Figure 1 illustrates the different adsorption sites, along with the adsorption energies according to the present model assumptions. Under these conditions, the Hamiltonian for N_B particles adsorbed on M sites can be written as

$$H = w_{AB} \sum_{\langle (i,j),(i',j') \rangle} c_{i,j} c_{i',j'} + w_{BB} \sum_{\langle (i,j),(i',j') \rangle} c_{i,j} c_{i',j'}, \qquad (1)$$

where $c_{i,j}$ is the occupation variable, which can take the following values: $c_{i,j} = 0$ if the corresponding site i, j is empty and $c_{i,j} = 1$ if the site is occupied. The first sum corresponds to the atoms on the surface of the NP only, and the second sum runs over the adsorbate sites. We consider only nearest neighbors interactions. Multiple occupations are not considered.

In a recent work [20] we have analyzed the problem of many-body interactions in detail. These simulations involved the use of many-body potentials and off-lattice models, which are expensive from a computational viewpoint. There, we have investigated silver deposition on gold NPs of truncated octahedral geometry for three different sizes in the grand canonical ensemble. A sequential deposition of adatoms on different facets was found, even in the case of a full vibrational picture. Remarkably, will see below that this problem may also be addressed by lattice models using pairwise additive interactions, obtaining qualitatively similar results.

The deposition process is simulated by a Monte Carlo technique in the grand canonical ensemble using the typical adsorption-desorption algorithm [21,22]. Thus, we consider the system in contact with a particle reservoir at temperature T and chemical potential μ. The Metropolis scheme [23,24] is used to satisfy the principle of detailed balance. A Monte Carlo step (MCS) is achieved when each of the M sites has been tested to change its occupancy state. Typically, the equilibrium state can be well reproduced after discarding the first 5×10^6 MCSs. Then, the next 2×10^6 MCSs are used to compute averages. Evaluations of different thermodynamic quantities follow standard procedures. The mean coverage, θ, is obtained as a simple average:

$$\theta(\mu) = \frac{\langle N_B \rangle}{M}. \qquad (2)$$

The differential heat of adsorption, q_d, is obtained from [25]:

$$q_d(\theta) = -\frac{\partial u}{\partial \theta} = \frac{\langle HN \rangle - \langle H \rangle \langle N \rangle}{\langle N^2 \rangle - \langle N \rangle^2}, \qquad (3)$$

where u is mean energy per site. The differential heat of adsorption is easily experimentally accessible by means of thermal desorption spectra. The physical interpretation of this quantity is the energy associated with the removal of a particle from the surface at a given coverage. Thus, thermal desorption spectra could be performed in order to check some of the predictions of the present modeling. Finally the thermodynamic factor, T_f,

$$T_f(\theta) = \left(\frac{\partial \beta \mu}{\partial \ln \theta} \right) = \frac{\langle N \rangle}{\langle (\delta N)^2 \rangle}, \qquad (4)$$

can be obtained either via the differentiation of adsorption isotherms [26] or via the normalized mean square fluctuations both obtained in grand canonical ensemble. The thermodynamic factor contains information on the fluctuation of the number of particles deposited on the NP. It is related to two experimental observables: the diffusion coefficient through the Darken equation and the isothermal susceptibility, χ, via the relationship $T_f = \theta/\chi$ [27,28].

The thermodynamic factor and the adsorption heat are quantities that emerge from the measurement of fluctuations in the system. It is of primary importance that their values

yield results in line with those stemming from the adsorption isotherms.

Different theoretical models available [29] allow the analytic estimation of adsorption isotherms on planar surfaces, such as, for example, the detailed mean field approximation (DMFA) and the effective substrates approximation (ESA) [30]. These models are based on a local description of the interaction between adsorbed particles and provide a qualitative description of the system. However, the prediction of quantities such as $T_f(\theta)$ and $q_d(\theta)$ is not possible without a previous computer simulation. The behavior of $q_d(\theta)$ has been analyzed for different systems in the case of planar surfaces [31], but their dependence on the shape and sizes of NPs has so far not been analyzed.

III. DISCUSSION

In Sec. III A we consider the effect of the different parameters of the model on the thermodynamic properties of an icosahedral nanoparticle made of 1415 atoms, ICO(1415). In Sec. III B the influence of icosahedra NP size is analyzed. In Sec. III C we analyze the behavior of other NP geometries and finally in Sec. III D we examine the spherical NP case.

A. Adsorption on ICO(1415)

We start the present analysis using a seed NP with $N_A = 1415$ with icosahedral geometry. We choose $k_BT = 1.0$ (k_B being the Boltzmann constant and T the temperature) and we define the energy ratio δE as $\delta E = w_{BB}/w_{AB}$, where we arbitrarily set $w_{BB} = -2.85$ (in units of k_BT) and w_{AB} is a parameter that will be given negative (attractive interactions) values with the condition $|w_{AB}| \leqslant |w_{BB}|$. At room temperature ($k_BT \approx 0.023$eV); the interactions selected correspond to values lying in a range that is intermediate between physical and chemical interactions. In Fig. 2(a), we present adsorption isotherms where the surface coverage θ is normalized according to Eq. (2) so that when $\theta = 1$, the surface of the NP is completely filled with B particles. For this coverage value, we will state that a complete monolayer has been formed. Two regimes can be distinguished to describe the system for the present NP size: regime I for $0 < \delta E \leqslant 1/3$ and regime II for $\delta E > 1/3$.

In regime I, the isotherm presents two well defined plateaus and an inflection in between, which is marked with an ellipse in Fig. 2(a). We note that the plateaus become wider as the interaction of the substrate with the adsorbate become relatively more important (as δE decreases). The case $\delta E = 0.0$ (not shown here) would correspond to the limiting case where lateral interactions are null (Langmuir-like adsorption). In this last situation only w_{AB} and the coordination of the adsorption site determine the heterogeneity of the adsorption process.

As discussed in the previous section, different types of adsorption sites are found on the NP. In the particular case of the icosahedral NPs, we can differentiate the faces, the edges, and the vertices, whose adsorption energies follow the sequence $E_{\text{face}} < E_{\text{edge}} < E_{\text{vertex}}$ (see Fig. 1). Thus, adsorbing

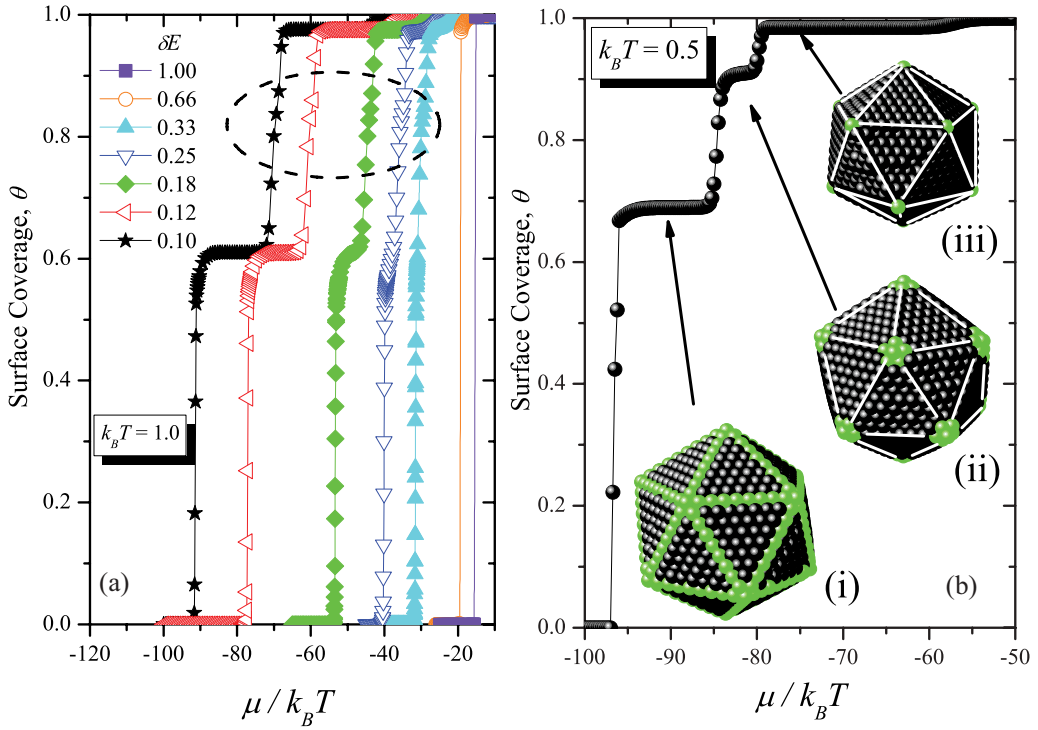

FIG. 2. (Color online) (a) Adsorption isotherms for several values of δE as indicated, at $k_BT = 1.0$. Regime I is associated with the occurrence of plateaus and regime II with a condensation. The ellipsoids show the onset of the second plateau. (b) Adsorption isotherm for $k_BT = 0.5$. The insets are snapshots of the states associated with each plateau. Black dots represent B particles, and green dots empty sites. The lines denote the geometry. In all cases $N_A = 1415$.

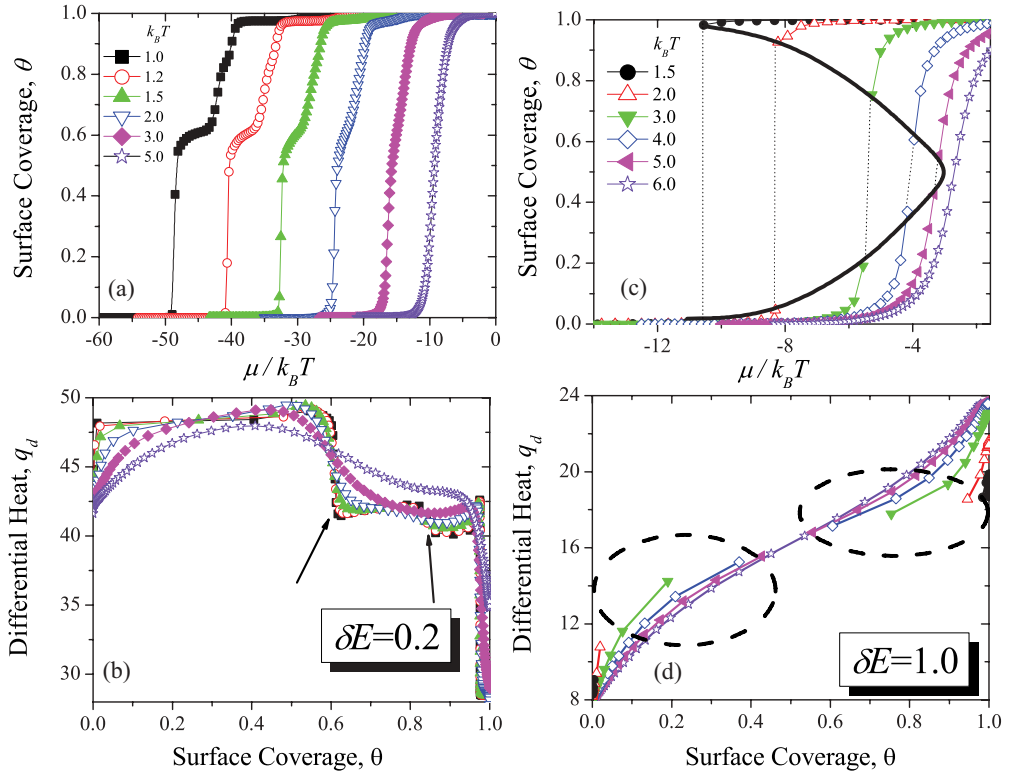

FIG. 3. (Color online) (a) Adsorption isotherms for $\delta E = 0.2$ in regime I for different k_BT values, as indicated in the figure. (b) Differential heat of adsorption versus surface coverage for the same conditions as in (a). Black arrows denote steps in the differential heat. (c) Regime II, for different k_BT values, as indicated in the figure, for $\delta E = 1.0$. The black line draws a possible diagram phase. (d) Differential heat versus surface coverage for the same temperature values as in (c). The ellipsoids mark the discontinuities of the curves. In all cases $N_A = 1415$.

particles prefer to first fill the faces, producing the first plateau. Following these ideas, the intermediate inflection corresponds to the filling of the edge sites. However, we note that this feature is very weak at $k_BT = 1.0$, becoming more evident at lower temperatures. Thus, the plateaus and the inflection denote different decoration types of the NP. At the beginning of deposition, when the NP is empty, the particles are deposited in a sequential manner, and they form nuclei for the growth of big islands that cover each one of the twenty faces of the icosahedron. In order to illustrate the previous deposition sequence, we present in the Fig. 2(b) representative snapshots of the configuration of the system at different stages of surface coverage for $\delta E = 0.2$ and $k_BT = 0.5$. Black and green spheres correspond to occupied and empty sites, respectively; the white lines are drawn to guide the eye. Inset (i) shows how B particles are deposited on the faces in the first plateau. In the second plateau, particles are deposited at the edge sites, as illustrated in inset (ii). Only the atoms around the vertices remain empty under these conditions. In the third plateau, the empty sites around the twelve vertices are filled [inset (iii)], and in a fourth plateau (not seen in the plot) the twelve sites at the vertices are finally filled.

Coming back to regime II, under these conditions each isotherm presents a discontinuity corresponding to the transition from an empty seed NP up to a fully covered surface [see two isotherms on the right of Fig. 2(a)]. Unlike in regime I, the deposition of B particles is not sequential in regime II, because the only way to minimize the energy is through full condensation. This behavior is typical for adsorption in two-dimensional arrays with attractive interactions, denoting the prevalence of the w_{BB} interactions over the w_{AB} ones. In the present regime, the morphology of the NP does not play a relevant role in determining the shape and position of the adsorption isotherm. Under these conditions, the latter is identical with that obtained for a (111) infinite surface.

Let us now analyze the temperature dependence of each regime. In Fig. 3(a) we explore regime I, choosing $\delta E = 0.2$ and varying the temperature from $k_BT = 1.0$ up to $k_BT = 5.0$. At high temperatures, the isotherms have the typical sigmoidal, Langmuir-like behavior. In this situation the interaction energy is less important than thermal fluctuations and the monolayer is formed in a single smooth transition showing no evidence of the energy topology of the surface. However, at low temperatures, the plateaus begin to be evident and become wider as k_BT decreases, corresponding to the most noticeable filling of the facets.

Another variable studied within regime I was the differential heat q_d as function of surface coverage, which was calculated according to Eq. (3). We note that alternatively q_d can be interpreted as the derivative of the mean energy per site with respect to surface coverage or as related with the fluctuation of the number of B particles. In this latter definition, we note further that q_d has steps at the coverages where the plateaus occur in the isotherms. This is more evident at the lower temperatures as is shown in Fig. 3(b) with arrows. However, as temperature increases, the steps begin to fade in the same

way as the plateaus do in the isotherms. At $k_BT \geqslant 3.0$ the first step in q_d can be barely noticed, and the second one disappears completely, in agreement with the observations made in Fig. 3(a) concerning the steps in the adsorption isotherm.

Figure 3(c) presents results for the adsorption isotherms in regime II. The condensation appears at different chemical potentials for each temperature. This characteristic resembles a first order phase transition between a surface phase with a low density and another one with a high density. As is usual for a first order transition, we can sketch the diagram phase by drawing a line through the discontinuity points along the isotherms. We can observe the typical symmetry of the diagram at half coverage. This behavior suggests the existence of a critical isotherm associated to a critical temperature, as in the case of a first order phase transition in a two-dimensional flat surface. At any temperature below this "critical temperature," the system prefers to condense in such a way that each adsorbed particle presents its nearest neighboring sites occupied, in contrast with a sequential deposition. At very high temperatures the isotherm becomes sigmoidal as before. Figure 3(d) shows the differential heats in this regime. At high temperatures the differential adsorption heat presents a smooth behavior as a function of the coverage, but at low temperatures it presents a discontinuity, as highlighted with an ellipsoid. Similarly to the case of the isotherms, the jumps in q_d depend on temperature.

Since the interactions in the present model are attractive, it is possible to assume a critical behavior at the formation of the first plateau, corresponding to condensation on the faces of the icosahedral NP. In order to analyze the isotherms at the first plateau, we choose $\delta E = 0.2$ and vary the temperature in Fig. 4. Like before, the isotherms show discontinuities corresponding to the transition from an empty lattice to covered faces. These jumps become more evident as temperature decreases. A possible diagram phase is shown by drawing a black line, presenting a maximum around $\theta \approx 0.33$, which

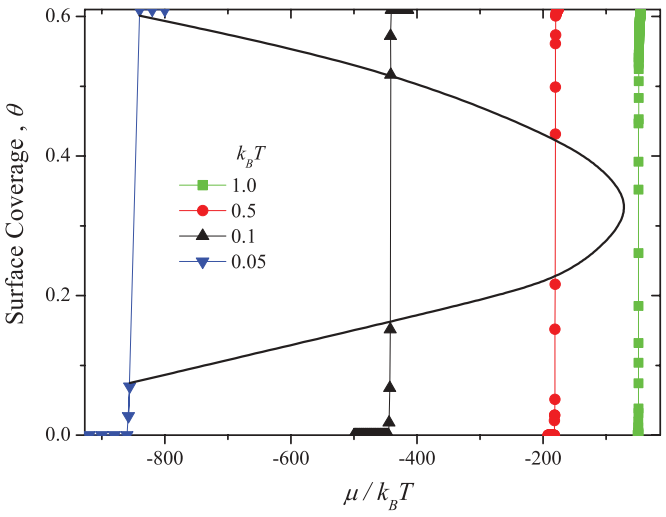

FIG. 4. (Color online) Adsorption isotherm, at different k_BT values as indicated in the figure. The jumps in the isotherms involve the condensation in the faces of the NP. The black line reconstructs a possible diagram phase.

corresponds to half of the full (111) facet coverage of the icosahedral NP.

B. Adsorption on icosahedral NPs of different sizes

The next point we consider is how NP size affects the thermodynamic adsorption variables, keeping its shape constant. It is well known that size is a very important factor affecting several processes in nanosystems. In Fig. 5(a), we present adsorption isotherms for icosahedra of different sizes, with N_A ranging between 561 and 10 179, at $k_BT = 1.0$ for $\delta E = 0.2$. In the case where $N_A = 561, 923$, and 1415, we can observe the occurrence of the first and the third plateaus only. The second plateau only becomes evident for $N_A \geqslant 2057$. The first plateau shows a remarkable size effect, because the number of face sites depends on N_A. It becomes broader as N_A increases; the black straight lines are drawn to guide the eyes. The inset shows a closeup of the third plateau; it can be observed that the width is the same for all sizes. This is not unexpected, since the number of vertex sites do not depend on N_A. An interesting dependence of differential heat on coverage is presented in Fig. 5(b). The process can be understood by focusing our attention on the steps. The first step is associated with the first plateau in the isotherm, where (111) faces are filled. The second step is associated with the deposition at the edges. It is remarkable that this step can be even observed for $N_A = 561$ (this is marked with an arrow), although there is no evidence for the occurrence of this phenomenon in the adsorption isotherm in Fig 5(a). The inset in Fig. 5(b) shows the q_d step related to the third plateau.

Another interesting variable that was examined is the thermodynamic factor, which is useful to calculate diffusion coefficients and is related to the second derivatives of the free energy. Figure 6(a) shows plots of T_f [Eq. (4)] versus surface coverage for different NP sizes with icosahedral geometry at $k_BT = 1.0$. The fluctuations in T_f have maxima for coverages where the plateaus occur in the isotherms and become enhanced as NP size increases. The most remarkable result is the shift of the three maxima with NP size. This is a typical "nano" effect, since in a macroscopic system all the maxima should occur at the same coverage. The behavior of a rounded maximum, corresponding to the second plateau, is shown in inset (i). Inset (ii) shows a closeup of a peak corresponding to the third plateau in θ, where we observe a behavior similar to the first one.

The effect of temperature on the behavior of T_f is shown in Fig. 6(b) for icosahedral NPs with $N_A = 1415$ and $\delta E = 0.2$. The sharp T_f maximum observed at relatively low temperatures becomes wider as temperature increases and finally disappears at $k_BT = 5.0$, as happened with the plateaus in the adsorption isotherms. These results show that at low temperatures, the lateral interactions at the faces are more intense than thermal fluctuations. The inset of Fig. 6(b) shows T_f in the coverage region corresponding to the third plateau.

From the analysis of the adsorption isotherms in Fig. 5(a), we observe that the coverage corresponding to the first and the second plateau, say θ_1 and θ_2, increase their value with N_A, moving towards the value of the third, say θ_3. Is there a limit for this shift? To answer this question, we can use the recurrence relations for the icosahedral geometry. With these relations we

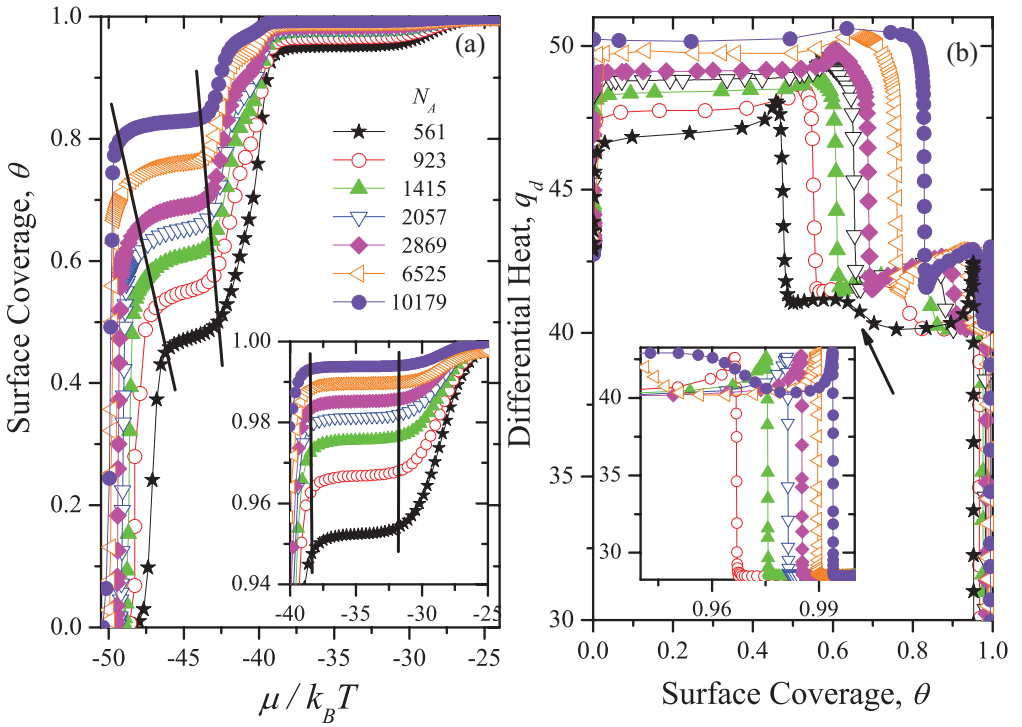

FIG. 5. (Color online) (a) Adsorption isotherms for different nanoparticle sizes N_A, as indicated in the figure. The inset shows a closeup of the third plateau. The black lines are a guide to the eye to show the change of the width of the plateaus. (b) Differential heats for the same conditions as in (a). The inset shows the step related to the third plateau. In all cases $k_B T = 1$.

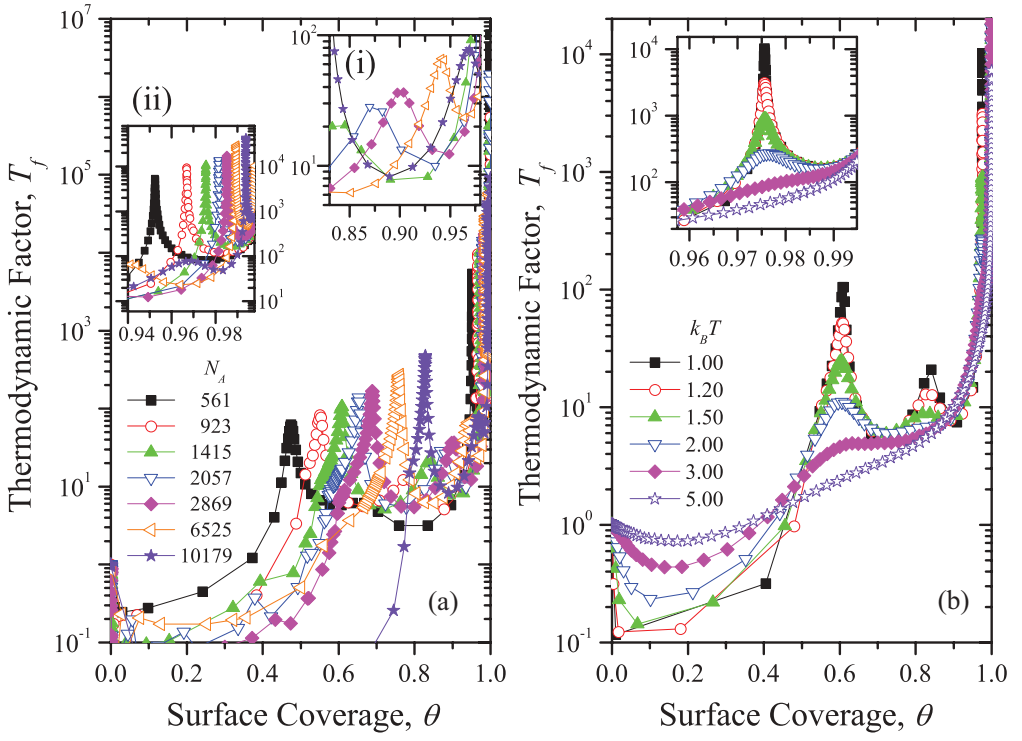

FIG. 6. (Color online) (a) Thermodynamic factor (T_f) versus surface coverage at $k_B T = 1$, for different nanoparticle sizes N_A as indicated in the figure. A peak occurs at each coverage degree where the plateaus are found in the isotherms. The inset shows two closeups of the second and third plateaus, respectively. (b) Temperature dependence of T_f. The maxima become sharper as the temperature goes down. The inset shows the T_f maxima corresponding to the third plateau.

TABLE I. Recurrence relations for the icosahedral geometry.

Vertex (N_v)	Edges (N_e)	Faces (N_f)	Bulk (N_b)
12	$30(n-1)$	$10(n^2-3n+2)$	$\frac{1}{3}(10n^3-15n^2+11n-2)$

can obtain the quantity of adsorption sites for each site type according to Table I:

In Table I n is a natural number that denotes the member of the icosahedral family to which the particle belongs. For example, for $n=1$ we get $N_T=13$, the smallest size for this kind of NP shape. Using the previous equations, the number of adsorption sites at the surface can be written as

$$N_B = 2(5n^2+1), \tag{5}$$

so, for the first, second, and third plateau the values of surface coverage can be calculated from

$$\theta_1 = \frac{N_f}{N_B} = \frac{5(n^2-3n+2)}{(5n^2+1)},$$
$$\theta_2 = \frac{N_f+N_e-5N_v}{N_B} = \frac{10n^2-70}{10n^2+2},$$
$$\theta_3 = \frac{N_f+N_e}{N_B} = \frac{10n^2-10}{10n^2+2}. \tag{6}$$

In θ_2 we have subtracted $5N_v$ sites, which correspond to the five nearest neighbors of the vertex sites. To check these expressions, we plot the coverage at which the three plateaus occur in the isotherms as a function of N_A in Fig. 7. The symbols correspond to the coverage of the plateaus from the simulations; the lines are the analytic expressions. All the analytic expressions present an asymptotic behavior. We observe a good agreement with the values of the simulation. The inset shows the surface coverage versus n. The third

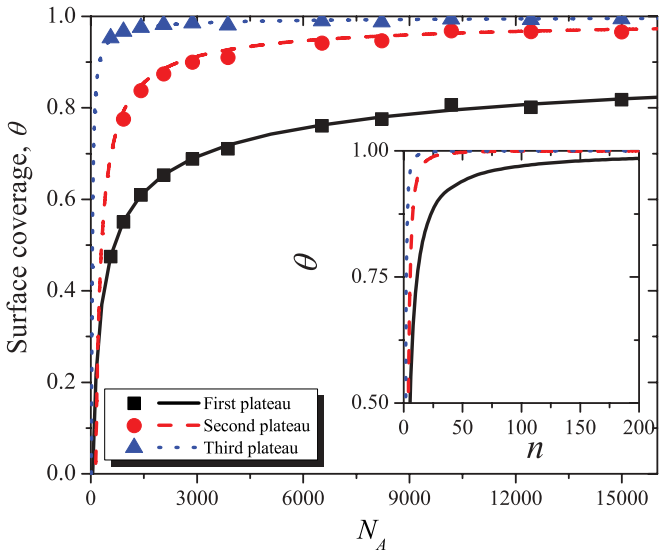

FIG. 7. (Color online) Coverage at the plateaus as a function of N_A. The symbols and lines represent the coverage from Monte Carlo simulations and theoretical expressions [Eq. (6)], respectively. The inset shows the coverages as a function of the index n defined in the text.

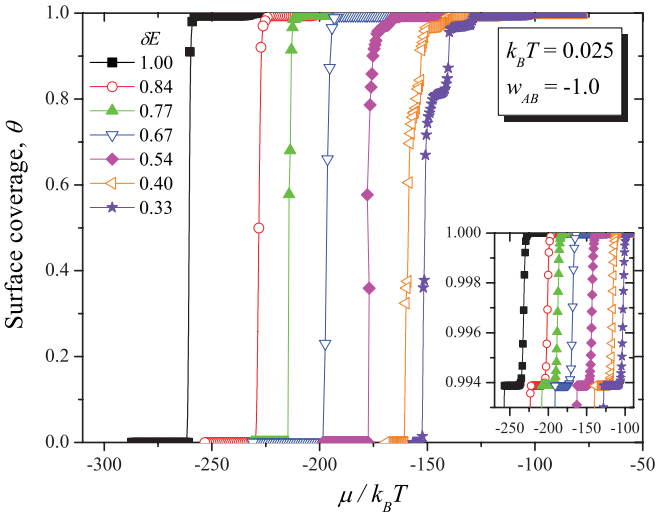

FIG. 8. (Color online) Adsorption isotherm for different values of δE at $T=300$K ($k_BT=0.025$). The inset shows a closeup of the third plateau. In all cases $N_A=10179$.

plateau appears for all values of $n>1$. On the other hand, the first and second plateau appear only for $n>3$ ($N_A>147$). This is because at $n>3$ there are more than one site on the faces. For small values of n the curves never cross, so that the plateaus always remain separate. However, at $n\approx 40$ the plateaus become close, and are difficult to separate from each other. Thus, the analytical expressions given above allow us to know the positions of the maxima in T_f versus N_A, as well as the location of the steps in the differential heat for all icosahedral NP sizes.

Now, we analyze the application of our model in a regime strictly valid for metallic interactions. Using the same definition for δE as before, we consider a NP with $N_A=10\,179$, setting $k_BT=0.025$ ($T=300$ K). In a first exploration we consider $w_{BB}=-1.0$, and vary the w_{AB} values in such a way that δE is in the range $3.0\leqslant\delta E\leqslant 1.0$. Under these conditions, the system presents characteristics similar to those found in regime II where the isotherms show discontinuities (these results are not shown here), resembling the behavior of an infinite surface. In a second exploration we set $w_{AB}=-1.0$ and vary the w_{BB} values in such a way that δE is in the range $1/3\leqslant\delta E\leqslant 1.0$, with the resulting isotherms shown in Fig. 8. For all values of energies we observe the occurrence of the third plateau. The inset shows a closeup in the third plateau region. At δE values close to 1, the isotherm present "jumps" and there is no evidence of others plateaus, but as δE approaches $\frac{1}{3}$ the others two plateaus begin to appear. In fact, in the isotherm corresponding to $\delta E=\frac{1}{3}$ three plateaus are evident. Their coverages are in agreement with the analytical values estimated above.

C. Adsorption on NP with different geometries

In the following we analyze the adsorption process on NP with different geometries. Figures 9(a)–9(c) shows the geometries considered in the present section: (a) truncated octahedron (TO), cuboctahedron (CO), and tetrahedron (TH). Other geometries like cubes, decahedra, and dodecahedra have

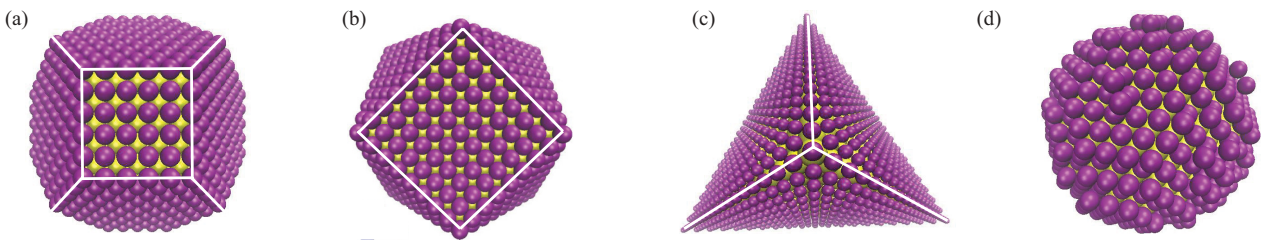

FIG. 9. (Color online) Representation of the different geometries of NP used in this work. The purple and yellow atoms correspond to the adsorbates and substrate, respectively. The edge and vertices sites are marked in white solid lines. (a) Truncate octahedral, (b) cuboctahedral, (c) prism, and (d) spherical.

been analyzed, but their qualitative behavior may be inferred from those mentioned above. For this reason we do not present these results. Figure 10(a) compares adsorption isotherms for ICO (blue) and CO (red) NPs for different δE values and $k_B T = 1$. For each member of the family, ICO and CO NPs present the same number of atoms, distributed in a different geometrical arrangement. In both cases, the plateaus in the isotherms become better defined as the interaction between A and B increases. The novel feature in the CO geometry is the occurrence of a fourth plateau, at more negative chemical potentials. The reason for this is the existence of (100) facets in the case of the CO NPs. The other three plateaus in CO NPs correspond to the phenomena already discussed for ICOs, that is, the filling of (111) facets, edges, and vertices. The latter two processes are advanced (occur at lower μs) in the case of ICOs, since the adsorption sites at edges and vertices exhibit a larger coordination than in COs.

Figure 10(b) shows that whatever the geometry of the NP (ICO, TO, CO, or TH), the filling sequence always presents the same behavior. In this case, for $\delta E = 0.1$ and $k_B T = 1$, the filling proceeds in the sequence (100) facets, (111) facets, edges, and vertices.

The general conclusion that we may draw from these simulations is that selective decoration of the different facets may be achieved, by choosing a suitable temperature, that obviously will depend on δE.

D. Spherical nanoparticles

Nanoparticles with perfect geometries as discussed in the previous sections are seldom found in experiments. On one side, sometimes it is found that different geometries are found within the same set of nanoparticles synthesized. On the other, domains with different crystallinities may be present in the

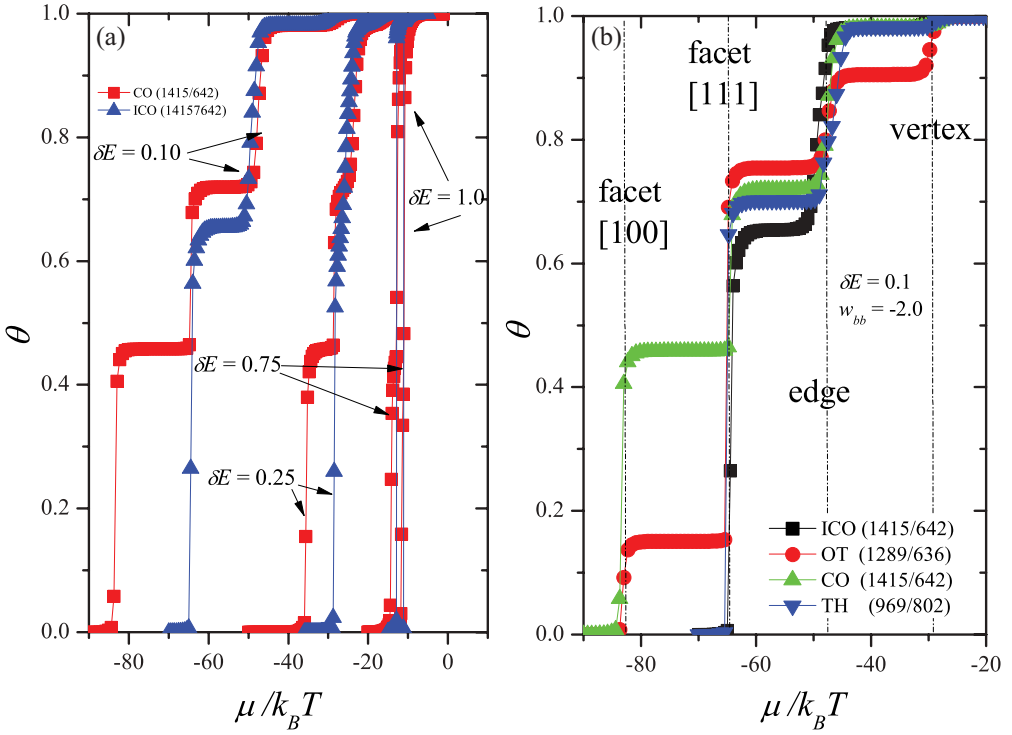

FIG. 10. (Color online) (a) Adsorption isotherms for several values of δE as indicated, at $k_B T = 1.0$ for cuboctahedra (black) and icosahedra (red) NP. (b) Adsorption isotherm for $\delta = 0.1$ and $k_B T = 1.0$ for different geometrical NP. Black: icosahedra, red: truncated octahedra, green: cuboctahedra, and blue: tetrahedron.

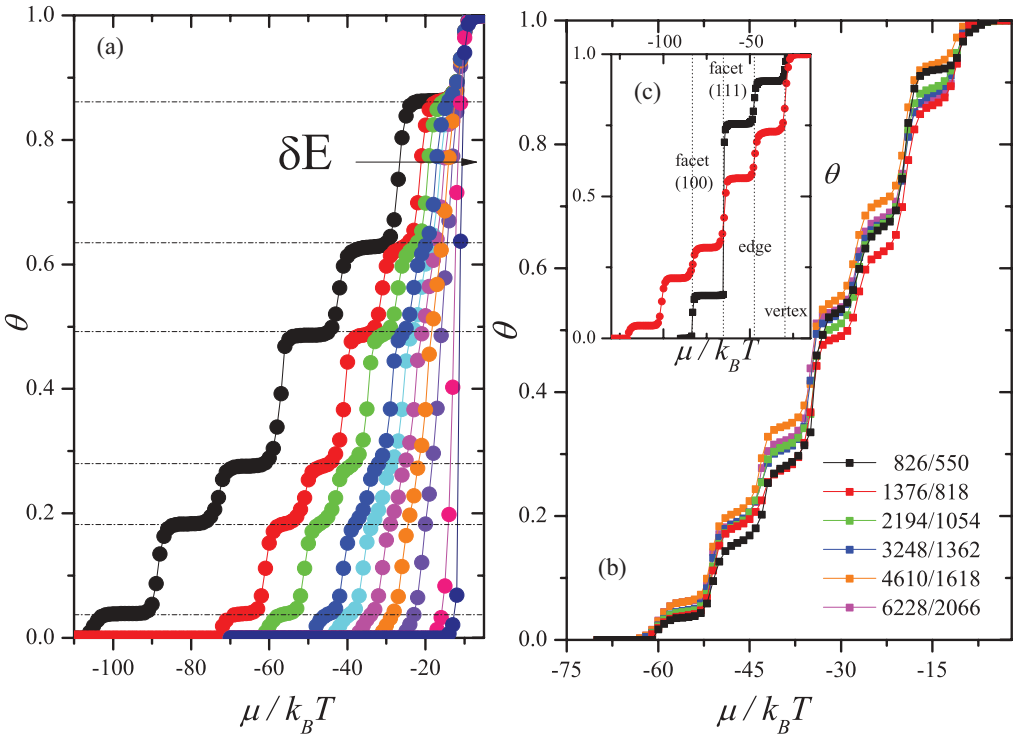

FIG. 11. (Color online) (a) Adsorption isotherms for several values of δE for spherical NP; $w_{BB} = -2.0$, $w_{AB} = -2.0, -2.66, -4.0, -5.0, -6.0, -7.0, -8.0, -10.0, -12.0, -15.0$. (b) Adsorption isotherm for $\delta = 0.5$ for different spherical size NPs. (c) Isotherms for spherical (black) and icosahedral (red) NPs. In all cases $k_B T = 1.0$.

same nanoparticle. Generally speaking, it is found that when the atomic arrangement of a real NP is compared with those given by perfect geometries (ICO, OT, CO, TO, etc.), the former presents a larger number of surface defects as extra borders, adatoms, vacancies, etc., where even these defects may assume different characteristics. Thus, the analysis and extrapolation of the theoretical predictions to a real NP is far from being straightforward. For example, if we assume a spherical shape for a NP, there is no definite recurrence relationship such as that given in Eq. (6) or similar. For this reason, in the following discussion we will choose the diameter as relevant parameter. The present choice to design a spherical nanoparticle was made on the basis of a bulk Au fcc structure, where different concentric spheres of radius R were employed to draw its limits. For example, a NP made of $N_A = 826$ atoms was constructed by choosing the atoms lying within a sphere of 2.42 nm diameter, which is a size of the order of those of the smallest ones of the NPs analyzed above. The next member of the spherical NPs was given a radius of 3.0 nm, which corresponds to the addition of a nearest neighbor distance between Au atoms, yielding a NP made of $N_A = 1376$ atoms. The difference $N_B = 550$ between both NPs defines the adsorbate lattice.

Figure 9(d) illustrates an image of the geometry discussed in the previous paragraph. Using the same methodology, we constructed six NPs with spherical geometry whose composition (N_A/N_B) is given by: 826/550, 1376/818, 2194/1054, 3248/1362, 4610/1618, and 6228/2066.

Figure 11(a) shows the adsorption isotherms for a 1376/818 spherical NP at different δE values at $k_B T = 1$. As in the case of the NPs with perfect geometries, depending on the relative interactions given by δE, there is a displacement of the curves towards more negative potentials and the plateaus turn to be better defined as the substrate-adsorbate interaction becomes stronger, $\delta E \to 0$. The last plateau, $\theta = 1$ in this figure, corresponds to the deposition of adsorbates on other previously adsorbed particles and would not be observed in experiment, since the related chemical potential region would correspond to the formation of the B bulk phase.

Figure 11(b) shows adsorption isotherms for spherical NPs of different sizes with $\delta E = 0.5$ and $k_B T = 1$. In contrast with the observation made in the case of NPs with a perfect geometry [Fig. 5(a)], no definite trend is found with NP size for the height step and plateau width, as it was, for example, for the case of Fig. 5(a).

Figure 11(c) compares isotherms for truncated octahedral (black) and spherical (red) NPs for the same values of δE and $k_B T$. In the first one, we can observe the steps corresponding to (100) facets, (111) facets, edges, and vertices. In the second, two new plateaus are evident at more negative chemical potentials. These correspond to the decoration of sites with a coordination of the substrate that is larger than 4. The analogies of these imperfections in planar surfaces are vacant sites, sometimes denominated zero-dimensional defects [32]. Thus, the results presented in Figs. 11(b) and 11(c) lead to the conclusion that the choice of a spherical shape for a nanoparticle leads to a relationship between sites of different coordination that remains relatively unaltered for different sizes.

In summary, our results show that the study of the deposition on NPs is a complex problem. The understanding and the

establishment of general rules in terms of the interaction between their constituents requires the consideration of NPs with different sizes and shapes. NPs with a perfect geometry such as icosahedra, octahedra, etc., present a more or less straightforward predictable behavior, which can be analyzed in terms of adsorption on sites with different coordinations. In contrast, spherical NPs do not present a clear-cut trend as a function of their size. Even more, adsorption isotherms appear to be rather size independent. The question is, what is the behavior expected in a real experiment? To answer this, we may think in terms of the two limiting cases considered in this work. A real NP will seldom have a perfect geometry, but it will have fewer defects than a spherical NP. Thus, the measurement of their properties will yield results between these two cases. The degree of approximation to one or another case could deliver an idea of how close the real system is to each of them.

IV. CONCLUSIONS

We have formulated a lattice model that can be used to study the thermodynamics of adsorbate formation on nanoparticles. This consists in a lattice gas that can be trivially extended to different geometries. The study of its properties was carried out through MC simulations in the grand canonical ensemble. The key parameter of the model was $\delta E = w_{BB}/w_{AB}$, that is, the ratio between the adsorbate-adsorbate and the substrate-adsorbate interactions. The properties calculated were adsorption isotherms, differential heats of adsorption, and thermodynamic factors. Depending on the values of the parameters, different types of behavior were found:

(1) In the case of icosahedral NPs for $k_BT = 1$ and $\delta\mathrm{E} \leqslant 1/3$, three plateaus in the adsorption isotherm occur that characterize the different deposition stages. Each plateau corresponds to configurations where sites of different types (faces, edges, and vertices) are filled. For $\delta\mathrm{E} > 1/3$, the isotherm presents a discontinuous behavior, corresponding to the transition from an empty icosahedral NP to a fully covered one. Other geometries show an increased number of plateaus (associated with different coordination of the adsorbates with the substrate) but exhibit the same qualitative behavior.

(2) Studies performed at different temperatures show smooth transitions or jumps in the isotherms, the latter corresponding to the transition from an empty NP to the full decoration of the NP. This behavior is a condensation, which resembles a first order phase transition in the case of infinite systems. The present results encourage a more detailed study on the critical behavior of the system.

(3) The effect of NP size on the thermodynamics variables was analyzed. Qualitative and quantitative aspects of shapes of the adsorption isotherms can be understood in terms of the geometry of the system. This is also valid for spherical NPs, where the shape of the isotherm is determined by the contribution of sites with different coordinations to the energetics of the system.

(4) When the ratio of adsorbate-adsorbate interactions to substrate-adsorbate interactions and the temperature is such that steps are observed in adsorption isotherms, the sequence of decoration depends on the coordination of adsorption sites, no matter what type of NP geometry is considered.

ACKNOWLEDGMENTS

We acknowledge financial support from CONICET PIP: 112-200801-000983, SECyT Universidad Nacional de Córdoba, Program BID (PICT-BICENTENARIO-2010-123), PME: 2006-01581, and CICYT-UNSE-CONICET.

[1] L. Gu, S. Cheley, and H. Bayley, Science **291**, 636 (2001).
[2] S. Coyle, M. C. Netti, J. J. Baumberg, M. A. Ghanem, P. R. Birkin, P. N. Bartlett, and D. M. Whittaker, Phys. Rev. Lett. **87**, 176801 (2001).
[3] X. F. Zhu and Z. G. Wang, Int. J. Nanotechnol. **3**, 492 (2006).
[4] T. L. Hill. *Thermodynamics of Small Systems (Parts I and II)* (Dover Publications, New York, 1994).
[5] T. L. Hill, Nano Lett. **1**, 273 (2001).
[6] L. N. Ferguson, Cell Biochem. Biophys. **11**, 11 (1987).
[7] O. A. Oviedo, E. P. M. Leiva, in *Metal Clusters and Nanoalloys: From Modeling to Applications*, Edited by M. M. Mariscal, O. A. Oviedo, and E. P. M. Leiva (Springer, Berlin, 2013).
[8] M. L. Personick, M. R. Langille, J. Zhang, and C. A. Mirkin, Nano Lett. **2011**, 3394 (2011).
[9] O. A. Oviedo, C. F. A. Negre, M. M. Mariscal, C. G. Sánchez, and E. P. M. Leiva, Electrochem. Commun. **16**, 1 (2012).
[10] See, for example, the articles published in Vol. 128 of Faraday Discuss. (2008).
[11] M. M. Mariscal, S. A. Dassie, and E. P. M. Leiva, J. Chem. Phys. **123**, 184505 (2005).
[12] M. M. Mariscal, N. A. Oldani, S. A. Dassie, and E. P. M. Leiva, Faraday Discuss. **138**, 89 (2008).
[13] O. A. Oviedo, E. P. M. Leiva, and M. M. Mariscal, Phys. Chem. Chem. Phys. **10**, 3561 (2008).
[14] E. V. Kovalyov and V. I. Elokhin, Chem. Eng. J. **154**, 88 (2009).
[15] E. V. Kovalev, V. I. Elokhin, A. V. Myshlyavtsev, and B. S. Bal'zhinimaev Doklady, Phys. Chem. **381**, 309 (2001).
[16] E. V. Kovalyov, V. I. Elokhin, and A. V. Myshlyavtsev, J. Comp. Chem. **29**, 79 (2007).
[17] E. V. Kovalyov, E. D. Resnyanskii, V. I. Elokhin, B. S. Bal'zhinimaeva, and A. V. Myshlyavtse, Phys. Chem. Chem. Phys. **5**, 784 (2003).
[18] K. Saha, K. Koga, and H. Takeo, Eur. Phys. J. D **9**, 539 (1999).
[19] Y. Wang, S. Teitel, and C. Dellago, Chem. Phys. Lett. **394**, 257 (2004).
[20] M. M. Mariscal, O. A. Oviedo, and E. P. M. Leiva, J. Mater. Res. **27**, 1777 (2012).
[21] K. Binder and D. Stauffer, in *Applications of the Monte Carlo*, Method in Statistical Physics, edited by K. Binder, Vol. 36 (Springer, Berlin, 1984).
[22] K. Kehr and K. Binder, in *Applications of the Monte Carlo Method in Statistical Physics*, Topics in Current Physics Vol. 36 (Springer, Berlin, 1987), p. 181.
[23] N. Metropolis, A. W. Rosenbluth, M. N. Rosenbluth, A. H. Tellery, and E. Teller, J. Chem. Phys. **21**, 1087 (1953).

[24] J. L. Soto, Ph.D. Thesis, University of Pennsylvania, 1979.
[25] D. Nicholson and N. G. Parsonage, *Computer Simulation and the Statistical Mechanics of Adsorption* (Academic Press, London, 1982).
[26] F. Nieto, C. Uebing, and Ber. Bunsenges, Phys. Chem. **102**, 156 (1998).
[27] J. W. Haus and K. W. Kehr, Phys. Rep. **150**, 263 (1987).
[28] R. Gomer, Rep. Prog. Phys. **53**, 917 (1990).
[29] F. Bulnes, A. J. Ramirez-Pastor, and G. Zgrablich, J. Chem. Phys. **115**, 1513 (2001).
[30] A. J. Ramirez-Pastor, D. Stacchiola, M. S. Nazarro, J. L. Riccardo, and G. Zgrablich, Surf. Sci. **449**, 43 (2000).
[31] M. C. Giménez, A. J. Ramirez-Pastor, and E. P. M. Leiva, Surf. Sci. **600**, 4741 (2006).
[32] E. Budevski, G. Staikov, and W. J. Lorenz, *Electrochemical Phase Formation and Growth* (Wiley-VCH, New York, 1996).